Catalytic Hydrogenation of Succinic Acid Using Materials of Fe/CeO₂, Cu/CeO₂ and Fe-Cu/CeO₂

Angela Ruiz, Claudia Castañeda,* Edwin Sosa, Carlos Rodríguez, Sonia Mancipe, José J Martínez,
María Helena Brijaldo, Hugo Rojas

Universidad Pedagógica y Tecnológica de Colombia, Escuela de Ciencias Química, Grupo de Catálisis-UPTC, Avenida Central de Norte, Vía Paipa, Boyacá, Tunja, Colombia

* Corresponding author's e-mail address: claudia.castaneda@uptc.edu.co

Abstract: The hydrogenation reaction of succinic acid in the liquid phase was studied using the supported metal catalysts, Fe/CeO₂, Cu/CeO₂, and Fe-Cu/CeO₂. The CeO₂ support was prepared by precipitation method and the supported metal solids by dry impregnation of support. For monometallic solids, a percentage of iron and copper of 10 wt.%, respectively, was considered. For the bimetallic solid, the metal content was 5 wt.% of each metal. The catalysts were characterized using atomic absorption spectroscopy, X-ray diffraction, nitrogen physisorption, and infrared spectroscopy techniques. The evaluation of the catalytic activity showed that the catalysts favor the formation of γ-hydroxybutyric acid (GHB), with the Cu/CeO₂ system presenting the highest percentages of conversion of succinic acid and yield towards GHB. This catalytic behavior could be related to the smaller crystallite size and the greater surface area evidenced in the material compared to the other catalysts studied. Furthermore, the results obtained using the bimetallic material evidenced the role of iron as a promoter for obtaining γ-butyrolactone (GBL).

Keywords: hydrogenation, succinic acid, γ-hydroxybutyric acid, Fe/CeO₂, Cu/CeO₂, Fe-Cu/CeO₂.

INTRODUCTION

RESEARCH on the use of renewable raw materials has increased in recent years to provide an alternative to the utilization of fossil resources. Among these sources is lignocellulosic biomass, which can be used to obtain various products such as succinic acid, glutamic acid, lactic acid, and levulinic acid, among others.[1] For this reason, succinic acid is considered a renewable resource with wide availability, and a platform chemical from which a variety of intermediate or final compounds with high added value can be obtained through hydrogenation, esterification, or amination reactions.[2–4] Among the aforementioned pathways, one of the most interesting is the hydrogenation of succinic acid (SA), primarily due to its potential reaction products, including γ-butyrolactone (GBL), 1,4-butanediol (BDO), and tetrahydrofuran (THF), which are used in the manufacture of polymers and industrial solvents.[5]

The hydrogenation of succinic acid is typically conducted in the liquid phase under high hydrogen pressures, employing supported metallic catalysts. These catalysts can be either monometallic, predominantly utilizing noble metals such as Pt, Rh, Pd, Ru, Re, or bimetallic, such as Pd-Re, Pd-Zr, Re-Ru, Ru-Sn, Pt-Re. They are commonly supported on activated carbon, TiO₂, Al₂O₃, SiO₂, or ZrO₂.[5–7] Table 1 presents a summary of succinic acid hydrogenation results using various heterogeneous catalysts, reaction conditions, and the corresponding yields obtained.[5,8–11]

As can be observed in Table 1, most of these studies report the use of 1,4-dioxane as a solvent; however, in some research, water has also been considered as a solvent, primarily because succinic acid produced by fermentation is obtained in the aqueous phase.[12–14] In the same vein, the literature reports different reaction pathways for the hydrogenation of succinic acid, depending mainly on the catalysts used. Figure 1 collects some of the pathways that the succinic acid hydrogenation process can follow and their corresponding products.

Several factors can influence the hydrogenation of succinic acid. The selectivity of the product can primarily be affected by the type of catalyst used and the reaction conditions.[13] Furthermore, a trend that has been observed is

Table 1. Studies on the catalytic hydrogenation of succinic acid.

Catalyst	Conversion SA / %	Yield / %	Reaction conditions	Solvent	Ref.
CuPd/SiO$_2$	100	86 (BDO)	200 °C / 80 bar / 96 h	1,4-dioxane	[5]
CuPd/γ-Al$_2$O$_3$	100	97 (THF)	200 °C / 80 bar / 96 h	1,4-dioxane	[5]
CuPd/TiO$_2$	73	66 (GBL)	200 °C / 80 bar / 96 h	1,4-dioxane	[5]
Re-Ru/MC	100	71 (BDO)	200 °C / 80 bar / 7 h	1,4-dioxane	[8]
Ir-Re/C	100	60-75 (THF)	240 °C / 150 bar / 10 h	Water	[9]
Pd/SiO$_2$-NH$_2$	100	94 (GBL)	240 °C / 60 bar / 4 h	1,4-dioxane	[10]
Ru/C	90	67 (GBL)	240 °C / 60 bar / 8 h	1,4-dioxane	[11]

that the main product obtained when using monometallic catalysts is GBL, whereas with bimetallic catalysts, the conversion of SA is facilitated, and the selectivity is directed towards BDO and THF.[5] Additionally, the addition of a second metal could minimize the use of precious metals.[16] For example, the use of Ru-Co bimetallic catalysts has proven to be advantageous for the selective production of BDO.[17]

Although the use of noble metals is suitable in these types of reactions, it tends to pose a disadvantage due to their scarcity and high prices, hence the need to replace them with other types of metals.[18] Some studies suggest the use of iron or copper, which are more abundant in the Earth's crust. In this regard, some researchers have reported the hydrogenation of succinic acid via dimethyl succinate (DMS) in the presence of methanol using a Re-Cu-MC catalyst, which favored a yield of 22.5 % towards GBL.[19] Meanwhile, utilizing Cu-Pd/HAP catalysts achieves an optimum yield towards BDO.[16] On the other hand, the Pd-Cu/AX catalyst has proven to be efficient for the selective production of GBL using isopropyl alcohol as a solvent.[1] Additionally, Liu et al. reported that the addition of Fe to the Pd-FeOx/C catalyst not only improved catalytic activity but also promoted the subsequent hydrogenolysis of GBL to BDO.[20]

Additionally, it is interesting to mention that, as evidenced in Figure 1, one of the stages involved in the hydrogenation of succinic acid can lead to a chemical equilibrium between γ-butyrolactone (GBL) and γ-hydroxybutyric acid (GHB), which generally depends on the reaction temperature and the pH of the solution.[21] GBL is commonly used as a solvent for polymers and alcohols, as well as for the removal of paints, lacquers, and adhesives, and as a raw material for pharmaceutical products.[22] Specifically, it serves as a starting compound in the synthesis of products such as *N*-methyl-2-pyrrolidone and 2-pyrrolidone, which are relevant in the pharmaceutical industry.[23]

On the other hand, GHB generally synthesized through the basic hydrolysis of GBL, is known to be a central nervous system depressant with unique pharmacological properties[24,25] and it is used in the treatments of narcolepsy[26] and for alcohol use disorder.[27] Additionally, its effectiveness has been demonstrated in improving the symptoms of fibromyalgia, alleviating pain, and fatigue, and restoring sleep.[28]

Considering the aforementioned points, this study investigated the hydrogenation reaction of succinic acid using monometallic and bimetallic catalytic materials of Fe/CeO$_2$, Cu/CeO$_2$, and Fe-Cu/CeO$_2$, aiming to analyze the catalytic behavior concerning the physical and chemical characteristics of these materials. Cerium dioxide (CeO$_2$) was chosen as the catalytic support due to its frequent use in various catalysis applications, either as a catalyst itself or as a support, owing to its structural and electronic properties. One of its most relevant characteristics is its ability to alternate between Ce(III) and Ce(IV) states through interaction with reducing or oxidizing substances.[29] These redox properties create a strong metal-support interaction,[30] making CeO$_2$-based catalysts an interesting option for selective hydrogenation reactions, as they could enhance catalytic activity.[31] Finally, iron and copper metals were chosen considering that there are currently no reports in the literature regarding their use in the studied reaction.
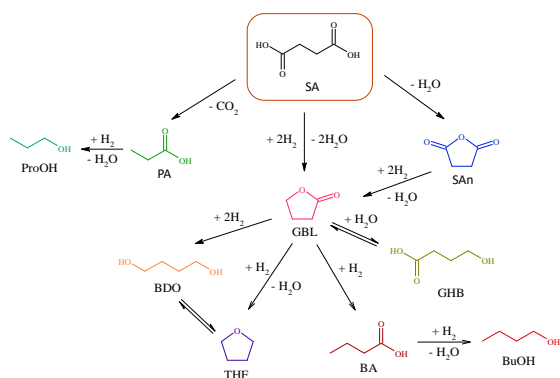
Figure 1. Main reaction pathways of succinic acid (SA) hydrogenation. Associated products include γ-butyrolactone (GBL), succinic anhydride (SAn), propionic acid (PA), propanol (ProOH), 1,4-butanediol (BDO), tetrahydrofuran (THF), γ-hydroxybutyric acid (GHB), butyric acid (BA), and butanol (BuOH). Adapted from.[7,15]

EXPERIMENTAL

Synthesis of the Catalysts

The catalytic support (CeO$_2$) was prepared using the precipitation method.[32] For this purpose, cerium nitrate hexahydrate (Ce(NO$_3$)$_3$·6H$_2$O, Sigma-Aldrich 99.5 %), sodium hydroxide (NaOH, Merck 99 %), and cetyltrimethylammonium bromide (CTAB, Alfa Aesar 98 %) were used as precursors. The procedure involved preparing a mixture in a beaker consisting of a 0.05 M solution of Ce(NO$_3$)$_3$ · 6H$_2$O and a 0.03 M solution of CTAB. Then, a 0.17 M solution of NaOH was added dropwise to the mixture, which was sealed and kept under constant stirring (300 rpm) at room temperature for 24 hours. Subsequently, a heat treatment was performed by refluxing the system at 90 °C for 3 hours with agitation, resulting in a yellow precipitate. The precipitate was filtered, washed with distilled water at 80 °C to remove traces of CTAB, and then dried at 100 °C for 6 hours. Finally, the solid was ground in an agate mortar to obtain a fine and homogeneous powder, which was then calcined at 450 °C for 4 hours using a ramp of 2 °C min^{-1}.

The supported metallic catalysts were synthesized using the dry impregnation method onto the support. The metallic precursors used were Cu(NO$_3$)$_2$ · 3H$_2$O and Fe(NO$_3$)$_3$ · 9H$_2$O. The procedure for obtaining the monometallic catalysts involved preparing an aqueous solution of the precursor with the necessary amount to achieve a 10 % mass content of metal. The solution was added dropwise to the support while constantly mixing, then subjected to thermal treatment at 110–120 °C for 8 h.

For the Fe-Cu/CeO$_2$ catalyst, the same procedure as for the monometallic catalysts described above was followed. In this case, the aqueous solution of Fe(NO$_3$)$_3$ · 9H$_2$O was first impregnated to achieve 5 % Fe by mass, followed by drying the material at 120 °C overnight. Subsequently, impregnation was carried out with the aqueous solution of Cu(NO$_3$)$_2$ · 3H$_2$O to obtain 5 % Cu by mass. Then, the Cu/CeO$_2$ solid was reduced at 400 °C, and the Fe/CeO$_2$ and Fe-Cu/CeO$_2$ catalysts were reduced at 700 °C for 2 h with a ramp rate of 4 °C min^{-1}.

Characterization of the Catalysts

The mass percentage of each metal present in the catalysts was determined using a Shimadzu AA 7000 flame atomic absorption spectrophotometer with air-acetylene flame. The wavelength for identifying Cu was 324.75 nm, and for Fe, it was 248.37 nm. Before to analysis, the samples underwent acid digestion in a reflux system for 1 hour at 250 °C with constant agitation. X-ray diffraction analyses were conducted to establish the degree of crystallinity of the catalysts, identify the crystalline phases present, and determine some structural data such as the average crystallite size and lattice parameters. The diffraction patterns were obtained using a Bruker D2 Phaser instrument. The solids were studied over the 2θ range of 5–80° with a step size of 0.6° s^{-1} and Cu Kα radiation (0.154 nm). The textural properties of the catalytic materials were analyzed using the N$_2$ physisorption technique at −196 °C on a Micromeritics ASAP 2020 porosimetry instrument. Prior to analysis, the samples were degassed at 250 °C for 4 hours to remove adsorbed molecules on the surface that could interfere with nitrogen adsorption. The calculation of the surface area of the catalysts was performed using the Brunauer-Emmet-Teller (BET) method. Additionally, the average pore size was determined using the Barrett-Joyner-Halenda (BJH) method applied to the desorption curve of the isotherms. The infrared spectra of the catalytic materials were obtained at room temperature using a Thermo Scientific Nicolet iS50 spectrometer equipped with an Attenuated Total Reflectance Fourier-Transform Infrared (ATR-FTIR) module. The wavenumber range studied was between 4000 and 500 cm^{-1} with a resolution of 4 cm^{-1} and 64 scans per sample.

Evaluation of the Catalytic Behavior

The hydrogenation reactions of succinic acid were carried out in a batch reactor using the Cu/CeO$_2$, Fe/CeO$_2$, and Fe-Cu/CeO$_2$ catalytic materials. For the hydrogenation reaction, 40 mL of a 0.1 M solution of succinic acid (PanReac AppliChem, 99 %) in 1,4-dioxane solvent was added to the reactor along with 50 mg of previously reduced catalyst. While adding the catalytic material, the solution was bubbled with nitrogen to prevent oxidation. The reactor was purged with N$_2$ and pressurized with H$_2$ initially at 600 psi, maintaining the temperature at 120°C with constant stirring at 700 rpm for 12 h. For reaction monitoring, samples were taken every 3 hours, filtered using a 0.45 μm cellulose membrane, and analyzed using a Varian 3800 gas chromatograph equipped with a flame ionization detector (FID). Helium was used as the mobile phase at a pressure of 15 psi, and the injector and detector temperatures were set at 250 °C. An RTX-5 column was employed. The catalytic activity of the materials was analyzed through the conversion (%C) of succinic acid, the selectivity (%S), and the yield (%Y) towards the products GBL and GHB ([Eq.(1)]–[Eq.(3)]).

$$\%C = \frac{n_{\text{SA initial}} - n_{\text{SA final}}}{n_{\text{SA initial}}} \times 100 \quad (1)$$

$$\%S = \frac{n_{\text{Product}}}{n_{\text{SA initial}} - n_{\text{SA final}}} \times 100 \quad (2)$$

$$\%Y = \frac{n_{\text{Product}}}{n_{\text{SA initial}}} \times 100 \quad (3)$$

RESULTS AND DISCUSSION

Characterization of the Catalysts

The results of the physicochemical characterization of the catalytic materials are presented below. Table 2 shows the percentages of each metal in the catalysts analyzed by atomic absorption spectroscopy. Considering that the experimental values are close to the nominal values, for the case of monometallic catalysts with 10 wt.% by mass of metal and for the bimetallic material with 5 wt.% Fe and 5 wt.% Cu, it can be mentioned that the dry impregnation method proves to be effective for the preparation of these types of catalysts.

The X-ray diffraction patterns obtained for both the synthesized support (CeO_2) and the supported catalysts of Fe/CeO_2, Cu/CeO_2, and $Fe-Cu/CeO_2$ are presented in Figure 2a. These were compared with the crystallographic charts from the Crystallography Open Database (COD).

All samples exhibit diffraction signals localized at 2θ angles of 28.2°, 32.8°, 47.2°, 56.1°, 58.8°, 69.2°, 76.7°, and 78.8° associated with the planes (111), (200), (220), (311), (222), (400), (331), and (420), respectively, corresponding to the fluorite-type cubic structure of CeO_2 (Cerianite, CeO_2, 9009008). Moreover, in the Cu/CeO_2 catalyst diffractogram, signals corresponding to copper can be identified at 2θ angles of 43.0° (111), 50.1° (200), and 73.9° (220) (Copper, Cu, 9013016). Additionally, in the Fe/CeO_2 catalyst diffraction pattern, a signal located at $2\theta = 44.5°$ (110) related to iron (Iron, Fe, 9013474) can be observed. However, in the diffractogram of the bimetallic catalyst, no additional signals corresponding to iron or copper are identified, which may be due to the low contents of the metals (5 wt.% Fe and 5 wt.% Cu).

In Figure 2b, an enlargement of the most intense signal related to the (111) plane of CeO_2 is shown, from which it can be determined that there is a slight displacement of the main diffraction signal. Thus, in catalysts containing iron, there is an increase in the diffraction angle compared to the position evidenced in the support, suggesting the possible inclusion of iron in the cerium dioxide lattice, considering that the ionic radius of Ce^{4+} (~ 0.97 Å) is larger than

that of Fe^{3+} (~ 0.68 Å); substitution of cerium by iron would generate slight changes in lattice parameters.[33] As shown in Table 2, Fe/CeO_2 and $Fe-Cu/CeO_2$ catalysts exhibit smaller edge lengths compared to the support lattice parameter. On the other hand, the addition of copper to cerium dioxide produces a slight displacement of the signal towards smaller diffraction angles (Figure 2b.). According to literature reports, the presence of Cu would help generate structural defects such as oxygen vacancies that promote the reduction of Ce^{4+} ions to Ce^{3+}. Considering that the ionic radius of Ce^{4+} is smaller than that of the Ce^{3+} ion,[34] this could explain the slight increase in the lattice parameter of the Cu/CeO_2 catalyst compared to the parameter of CeO_2.[35]

Additionally, the X-ray diffraction results allow for the observation of significantly more intense and narrower signals for materials containing iron, compared to the signals observed in the support. Therefore, considering that the average width of the diffraction signal is related to the crystallite size, the Scherrer equation was employed to calculate this parameter, obtaining the results recorded in
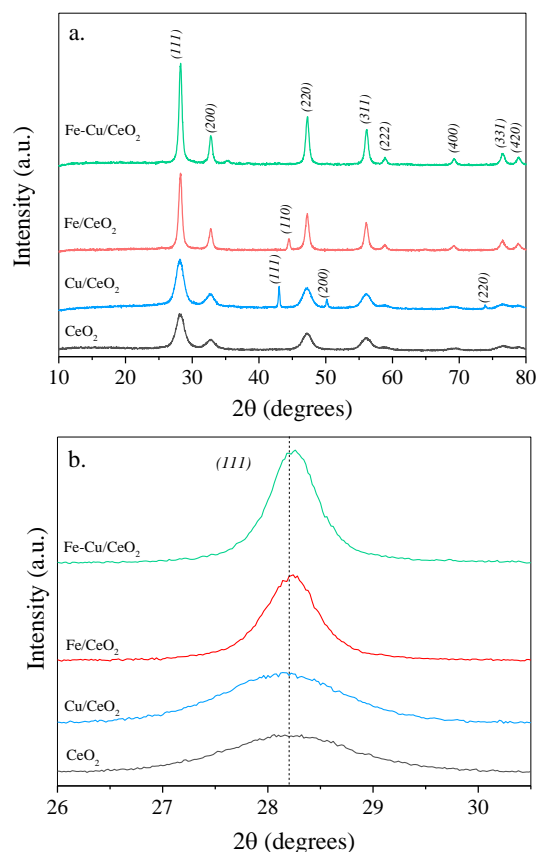
Figure 2. a) X-ray Diffractogram of the support and the catalysts. b) Magnification of the diffraction signal corresponding to plane (111).

Table 2. Structural parameters of the catalysts.

Catalyst	Metal content		Cristallite size / nm	Lattice parameters / nm	SBET / $m^2\,g^{-1}$	Pore Size
	%Fe	%Cu				
CeO_2	-	-	6.2	0.5476	156	4.6
Cu/CeO_2	-	8.5	10.3	0.5488	103	5.2
Fe/CeO_2	8.8	-	13.3	0.5473	12.0	49
$Fe-Cu/CeO_2$	4.7	4.8	14.8	0.5469	11.2	54

Table 2, confirming an increase in the crystallite size of the catalysts containing iron compared to that calculated in the support. It is worth mentioning that the Cu/CeO_2 catalyst also exhibits an increase in crystallite size, although to a lesser extent than in the catalysts with iron content.

The surface texture of the catalysts and the prepared support was studied using nitrogen adsorption-desorption isotherms, which are shown in Figure 3a.

Taking into account the classification of physisorption isotherms assigned by the IUPAC,[36] it can be observed that all analyzed samples exhibit type IV adsorption-desorption isotherms (a), related to mesoporous solids, characterized by the formation of a hysteresis loop due to irregular capillary condensation. In the case of CeO_2 and the Cu/CeO_2 catalyst, an H2-type hysteresis is generated at relative pressures between 0.41 and 0.92, corresponding to pores with a "bottle-neck" shape. On the other hand, the Fe/CeO_2 and $Fe-Cu/CeO_2$ catalysts exhibit H3-type hysteresis at high relative pressures between 0.88 and 0.99, characterized by slit-like flexible pores which can occur when the pore network contains macropores that are not filled.
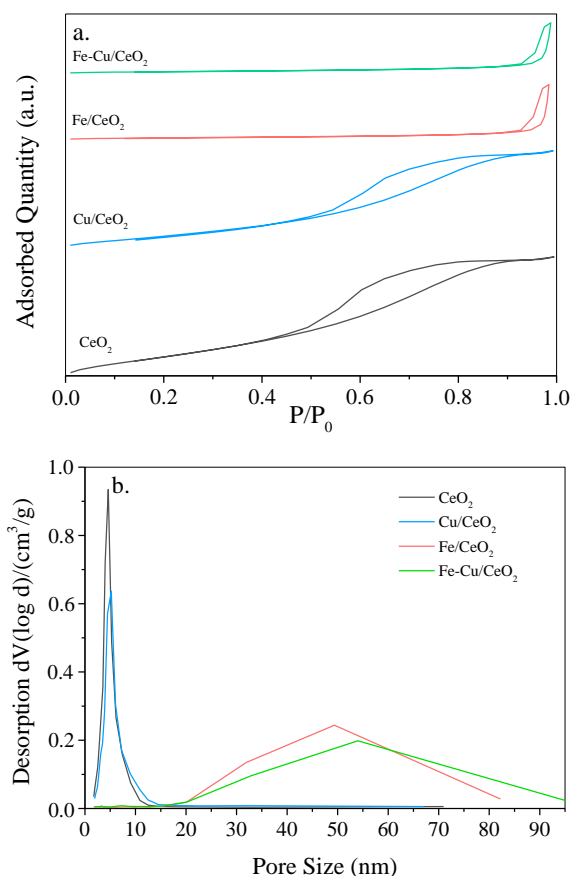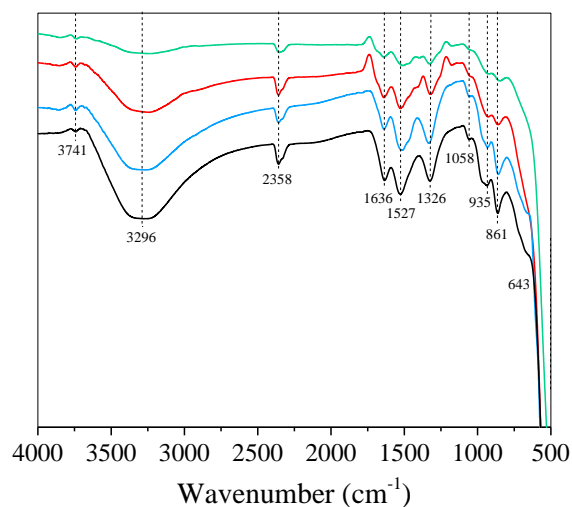
In Table 2, the results of specific surface area (S_{BET}) and pore size for the support and the prepared catalysts are presented. The specific surface area was determined using the Brunauer-Emmett-Teller (BET) method, obtaining an area of 156 m^2 g^{-1} for CeO_2. The impregnation of a metal onto the support decreases the specific surface area, resulting in low values such as those observed for the $Fe-Cu/CeO_2$ catalyst at 11.2 m^2 g^{-1}. These results suggest that this textural property decreases as a result of potential pore blockage by the metals on the surface of CeO_2.

The average pore size distribution of the catalysts is shown in Figure 3b., determined using the Barrett-Joyner-Halenda (BJH) method. From the results obtained, it can be observed that the analyzed materials exhibit a monomodal pore distribution with different sizes. The support and the Cu/CeO_2 catalyst have pore sizes of 4.6 and 5.2 nm, respectively, while in the monometallic and bimetallic iron catalysts, the pore size increases considerably (49 and 54 nm, respectively). This correlates with the pore volume obtained, the specific surface area, and the crystallite size. Higher crystallinity involves larger crystals, resulting in smaller extents of surface areas. As demonstrated earlier, the supported materials have larger crystallite sizes than the CeO_2, justifying the obtained area values.

The ATR-FTIR spectra of CeO_2 and the catalysts studied can be observed in Figure 4. All analyzed materials present a small band around 3741 cm^{-1} corresponding to isolated hydroxyl groups. Near 3296 cm^{-1}, broadband can be observed in all samples, attributed to the stretching vibrations of the O−H bond of surface-adsorbed water molecules; furthermore, a signal can be observed around 1636 cm^{-1} assigned to the scissoring-type bending vibration of the hydroxyl group,[37] and at 1527 cm^{-1} and 935 cm^{-1}, bands related to the stretching vibrations of the O−H

Figure 3. a) Adsorption-desorption isotherms of the catalysts. b) Average pore size distribution of the catalysts.

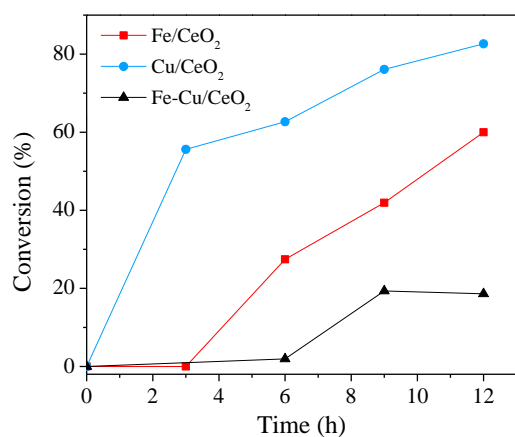**Figure 4.** Infrared spectra of the catalysts studied.

bond.[38,39] It is noteworthy that these signals are less intense in the Fe-Cu/CeO$_2$ catalyst, indicating a less hydroxylated surface in this solid compared to the other catalytic materials.

On the other hand, the band at 1326 cm^{-1} is attributed to Ce-O-Ce stretching vibrations,[40] and characteristic signals of Ce-O stretching vibrations can be observed at 861 cm^{-1} and 643 cm^{-1}.[41] Finally, the bands at 2358 cm^{-1} and 1058 cm^{-1} are due to the stretching vibrations of adsorbed CO$_2$ molecules in the samples.[42]

Evaluation of the Catalytic Behavior

Figure 5 shows the percentage of succinic acid conversion over 12 h of reaction with each catalytic material. The Cu/CeO$_2$ catalyst exhibited higher conversion compared to the other materials, reaching a value of 55.6 % within the first 3 h and showing a progressive increase over time. In contrast, the Fe/CeO$_2$ and Fe-Cu/CeO$_2$ catalysts showed lower conversions after 12 hours (60 % and 18.6 %, respectively). Additionally, the time required to perceive an increase in conversion was longer, especially in the case of the bimetallic catalyst.

On the other hand, monitoring the reaction allowed us to observe the formation of γ-butyrolactone (GBL) and γ-hydroxybutyric acid (GHB) as the main reaction products. In Figures 6 a–c., the yield obtained for the two products GBL and GHB at 12 h of reaction using the synthesized catalytic materials can be observed. All catalysts tend to show a greater favorability towards the formation of GHB. In the case of the Cu/CeO$_2$ catalyst, the best results were obtained in terms of the yield of the main product, with a value of 78.3 %, while very small percentages are observed for GBL. For the Fe/CeO$_2$ material, there is an increase in yield towards GBL with a maximum value of 9.4 %; however, the

percentages for GHB decrease when compared to the monometallic copper catalyst. The Fe-Cu/CeO$_2$ bimetallic system showed the lowest yield towards GHB of all; however, it is worth noting that the percentage of GBL obtained with this catalyst is higher than that achieved with Cu/CeO$_2$, but lower when compared to the yield of Fe/CeO$_2$ for this product after 12 h of reaction.
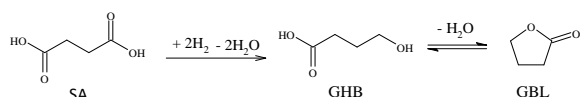

Figure 5. Succinic acid conversion over time for each catalyst.
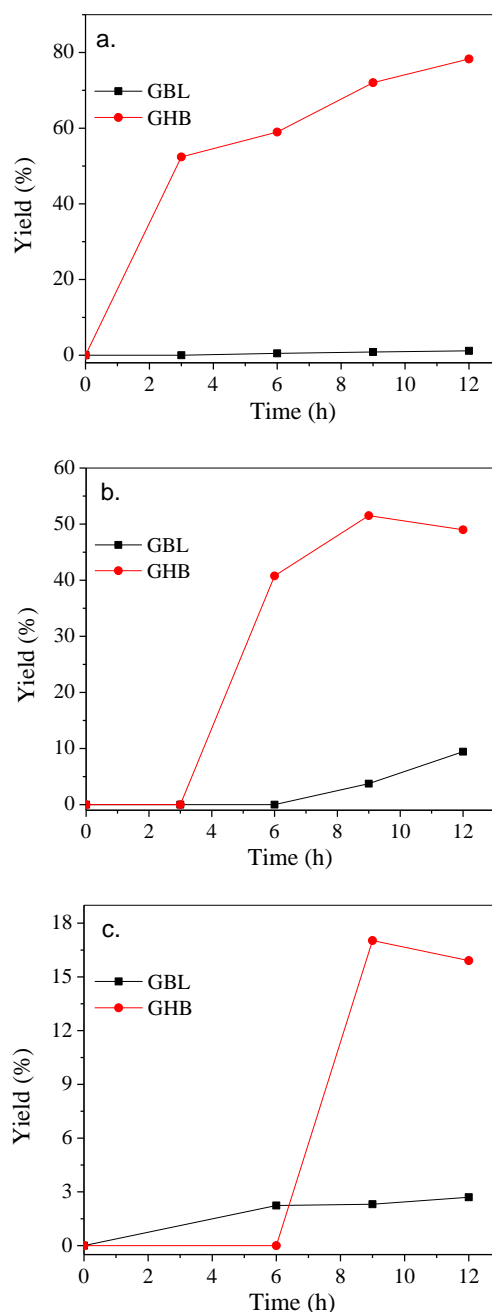
Figure 6. Yield obtained to GBL and GHB at 12 h of reaction using a) Cu/CeO$_2$, b) Fe/CeO$_2$, c) Fe-Cu/CeO$_2$.

In Table 3, a compilation of the most relevant data regarding the catalytic activity of the catalysts in the hydrogenation reaction of succinic acid can be observed. From this information, it can be noted primarily that the selectivity of all catalysts was directed towards GHB, and the highest conversion was obtained with the Cu/CeO$_2$ catalyst. Additionally, other products were generated, the identification of which was not possible to perform.

Based on the results obtained, it can be observed that the physicochemical characteristics of the catalysts influenced the conversion percentages and yields obtained in the hydrogenation of succinic acid. In this way, it can be stated that iron and copper catalytic materials supported on cerium oxide are conducive to the formation of GHB. However, the Cu/CeO$_2$ catalyst presented some structural and textural properties different from those determined for the Fe/CeO$_2$ and Fe-Cu/CeO$_2$ materials, which could be correlated with the disparities in their catalytic behavior. Therefore, the increase in conversion and, likewise, the percentage of yield towards GHB was influenced by textural and structural parameters. Thus, the monometallic copper catalyst exhibited the best catalytic performance in the reaction, probably related to its higher surface area, smaller pore size, and crystallite size compared to the other catalytic materials studied in the reaction.[11] On the other hand, the bimetallic catalyst showed the lowest values in terms of conversion and yield, which correlates with its lower surface area and larger pore size. Finally, iron acted as a promoter for the production of GBL, as better yields towards this product were obtained with the bimetallic material compared to the result observed when conducting the reaction in the presence of monometallic copper material.

Finally, the hydrogenation of succinic acid primarily led to the formation of GHB as the main product of the reaction in the presence of the three studied catalysts. However, the formation of GBL was also detected. Therefore, the reaction pathway involves initially the reduction of one of the two carboxyl groups of succinic acid to form GHB, followed by an intramolecular dehydration of this compound, leading to the formation of GBL, as shown in Figure 7.

Although the conversions achieved in the present study are slightly lower than those obtained in studies focused on the use of supported noble metal catalytic materials, principally based on Pd (see Table 1)[5,10] it is important to highlight the usefulness of Cu/CeO$_2$ materials for obtaining the GBH product. It has been observed that GHB can be formed from the initial times on metal supported on basic catalysts[10] and is further dehydrated to form GBL. Commonly, GBL formation to GHB occurs due to the cleavage of the lactone ring in an acidic medium.[21]

It is worth mentioning that the selective hydrogenation of succinic acid is a significant challenge currently under investigation. This is because this type of reaction is primarily hindered in carboxylic acids due to the low electrophilicity associated with the polarization of the carbonyl carbon.[9] However, the results of this study highlight the potential use of supported catalytic materials based on the use of widely available metals such as iron and copper.

CONCLUSIONS

The modification of the cerium oxide support through the dry impregnation of metals such as copper and iron induced changes in the textural and structural properties of CeO$_2$ reflected in a reduction of the surface area and an increase in crystallite size. These parameters influenced the catalytic behavior observed in the monometallic and bimetallic catalysts studied in the hydrogenation reaction of succinic acid. In the presence of the examined catalysts, the formation of GHB and GBL as the main reaction products was promoted. It was observed that all materials exhibited high selectivity towards GHB, with the Cu/CeO$_2$ catalyst achieving the best conversion (82.7 %) and yield (78.3 %). These catalytic performance results are correlated with the physicochemical characteristics of the catalysts, as smaller crystallite size and larger surface area resulted in better yields and conversions.

Table 3. Results of the Catalytic activity using the materials studied in the succinic acid hydrogenation.

Catalyst	Conversion / %	Yield / %		Selectivity / %		
		GBL	GHB	GBL	GHB	Others
Cu/CeO$_2$	82.7	1.2	78.3	1.5	94.7	3.8
Fe/CeO$_2$	60.0	9.4	49.0	15.7	81.7	2.6
Fe-Cu/CeO$_2$	18.6	2.7	15.9	14.5	85.5	0.0

Figure 7. Reaction pathway for the hydrogenation of succinic acid in the presence of Cu/CeO$_2$, Fe/CeO$_2$, and Fe-Cu/CeO$_2$ catalysts. Adapted from.[10]

REFERENCES

[1] S. Patankar, A. Sharma, G. Yadav, *Clean Technol. Environ. Policy*. **2018**, *20*, 683–693. https://doi.org/10.1007/s10098-017-1381-6

[2] A. Corma, S. Iborra, A. Velty, *Chem. Rev.* **2007**, *107*, 2411–2502. https://doi.org/10.1021/cr050989d

[3] C. Delhomme, S. L. M. Goh, F. E. Kühn, D. Weuster-Botz, *J. Mol. Catal. B Enzym.* **2012**, *80*, 39–47. https://doi.org/10.1016/j.molcatb.2012.03.010

[4] M. O. Haus, Y. Louven, R. Palkovits, *Green Chem.* **2019**, *21*, 6268–6276. https://doi.org/10.1039/C9GC01488H

[5] S. D. Le, S. Nishimura, *Appl Catal B: Environ*. **2021**, *282*, 119619. https://doi.org/10.1016/j.apcatb.2020.119619

[6] R. Luque, J. H. Clark, K. Yoshida, P. L. Gai, *Chem. Commun.* **2009**, *35*, 5305–5307. https://doi.org/10.1039/b911877b

[7] C. Heisig, J. Diedenhoven, C. Jensen, H. Gehrke, T. Turek, *Chem. Eng. Technol.* **2020**, *43*, 484–492. https://doi.org/10.1002/ceat.201900324

[8] K. H. Kang, U. G. Hong, Y. Bang, J. H. Choi, J. K. Kim, J. K. Lee, S. J. Han, I. K. Song, *Appl. Catal. A: Gen.* **2015**, *490*, 153–162. https://doi.org/10.1016/j.apcata.2014.11.029

[9] J. M. Keels, X. Chen, S. Karakalos, C. Liang, J. R. Monnier, J. R. Regalbuto, *ACS Catal.* **2018**, *8*, 6486–6494. https://doi.org/10.1021/acscatal.8b01006

[10] C. You, C. Zhang, L. Chen, Z. Qi, *Appl. Organomet. Chem.* **2015**, *29*, 653–660. https://doi.org/10.1002/aoc.3342

[11] U. G. Hong, H. W. Park, J. Lee, S. Hwang, I.K. Song, *J. Ind. Eng. Chem*. **2012**, *18*, 462.

[12] B. K. Ly, B. Tapin, F. Epron, C. Pinel, C. Especel, M. Besson, *Catal. Today*. **2020**, *355*, 75–83. https://doi.org/10.1016/j.cattod.2019.03.024

[13] Z. Shao, C. Li, X. Di, Z. Xiao, C. Liang, *Ind. Eng. Chem. Res.* **2014**, *53*, 9638–9645. https://doi.org/10.1021/ie5006405

[14] B. Tapin, F. Epron, C. Especel, B. K. Ly, C. Pinel, M. Besson, *ACS Catal.* **2013**, *3*, 2327–2335. https://doi.org/10.1021/cs400534x

[15] A. Küksal, Einstufige Synthese von 1,4-Butandiol durch Hydrierung von Maleinsäureanhydrid in der Flüssigphase, **2006**.

[16] S. D. Le, S. Nishimura, *ACS Sustain. Chem. Eng.* **2019**, *7*, 18483–18492. https://doi.org/10.1021/acssuschemeng.9b04447

[17] P. K. Baidya, U. Sarkar, R. Villa, S. Sadhukhan, *BMC chem. eng.* **2019**, *1*, 10. https://doi.org/10.1186/s42480-019-0010-z

[18] M. Abou Hamdan, S. Loridant, M. Jahjah, C. Pinel, N. Perret, *Appl. Catal. A: Gen.* **2019**, *571*, 71–81. https://doi.org/10.1016/j.apcata.2018.11.009

[19] K. H. Kang, U. G. Hong, J. O. Jun, J. H. Song, Y. Bang, J. H. Choi, S. J. Han, I. K. Song, *J. Mol. Catal. A Chem.* **2014**, *395*, 234–242. https://doi.org/10.1016/j.molcata.2014.08.032

[20] X. Liu, X. Wang, G. Xu, Q. Liu, X. Mu, H. Liu, *J. Mater. Chem. A.* **2015**, *3*, 23560–23569. https://doi.org/10.1039/C5TA03843J

[21] M. T. Pérez-Prior, J. A. Manso, M. del Pilar García-Santos, E. Calle, J. Casado, *J. Org. Chem.* **2005**, *70*, 420–426. https://doi.org/10.1021/jo040271i

[22] J. A. Lee, J. H. Ahn, S. Y. Lee (**2019**) 2019, pp. 172.

[23] J. H. Jang, M. Abu-Omar, *Energies*. **2020**, *13*, 6402. https://doi.org/10.3390/en13236402

[24] S. A. León, Clinical pharmacology and abuse potential of gamma-hydroxybutyric acid (GHB), **2008**.

[25] M. Blumenfeld, R.G. Suntay, M.H. Harmel, *Anesth. Analg.* **1962**, *41*, 721–726. https://doi.org/10.1213/00000539-196211000-00011

[26] G. Mayer, *Expert Rev. Neurother.* **2012**, *12*, 519–529. https://doi.org/10.1586/ern.12.42

[27] F. Caputo, T. Vignoli, C. Tarli, M. Domenicali, G. Zoli, M. Bernardi, G. Addolorato, *Int. J. Environ. Res. Public. Health.* **2016**, *13*, 290. https://doi.org/10.3390/ijerph13030290

[28] R. Staud, *Expert opinion on pharmacotherapy*. **2011**, *12*, 1789–1798. https://doi.org/10.1517/14656566.2011.589836

[29] J. Kammert, J. Moon, Z. Wu, *Chin. J. Catal.* **2020**, *41*, 901–914. https://doi.org/10.1016/S1872-2067(19)63509-6

[30] J. Beckers, G. Rothenberg, *Green Chem*. **2010**, *12*, 939–948. https://doi.org/10.1039/c000191k

[31] K. Razmgar, M. Altarawneh, I. Oluwoye, G. Senanayake, *Catal. Surv. Asia.* **2021**, *25*, 27–47. https://doi.org/10.1007/s10563-020-09319-z

[32] H.-Q. Li, X. Liu, Q. Zhang, S.-S. Li, Y.-M. Liu, H.-Y. He, Y. Cao, *Chem. Commun.* **2015**, *51*, 11217–11220. https://doi.org/10.1039/C5CC03134F

[33] P. Sudarsanam, B. Mallesham, D. N. Durgasri, B. M. Reddy, *RSC Adv.* **2014**, *4*, 11322–11330. https://doi.org/10.1039/C3RA45778H

[34] S. Adak, R. S. Pal, T. S. Khan, M. K. Poddar, M. S. Ahmad, V. V. D. N. Prasad, M. A. Haider, R. Bal, *ChemistrySelect*. **2021**, *6*, 13051–13059. https://doi.org/10.1002/slct.202102859

[35] S. T. Hossain, E. Azeeva, K. Zhang, E. T. Zell, D. T. Bernard, S. Balaz, R. Wang, *Appl. Surf. Sci.* **2018**, *455*, 132–143. https://doi.org/10.1016/j.apsusc.2018.05.101

[36] M. Thommes, K. Kaneko, A. V. Neimark, J. P. Olivier, F. Rodriguez-Reinoso, J. Rouquerol, K. S. W. Sing, *Pure. Appl. Chem.* **2015**, *87*, 1051–1069. https://doi.org/10.1515/pac-2014-1117

[37] Y. H. Liu, J. C. Zuo, X. F. Ren, L. Yong, *Metalurgija*. **2014**, *53*, 463.

[38] M. Ramachandran, R. Subadevi, M. Sivakumar, *Vacuum*. **2019**, *161*, 220–224. https://doi.org/10.1016/j.vacuum.2018.12.002

[39] T. Thuy, D. Duong, N. Vi, D. Nguyên, T. Thinh, N. Bang, P. Vuong, M. Nguyen N, *Bull. Chem. React. Eng.* **2022**, *17*, 554–564. https://doi.org/10.9767/bcrec.17.3.15384.554-564

[40] G. Bai, J. Wang, Z. Yang, H. Wang, Z. Wang, S. Yang, *RSC Adv*. **2014**, *4*, 47096–47105. https://doi.org/10.1039/C4RA09488C

[41] B. Jain, A.K. Singh, A. Hashmi, M.A.B.H. Susan, J.-P. Lellouche, *Adv. Compos. Hybrid. Mater.* **2020**, *3*, 430–441. https://doi.org/10.1007/s42114-020-00159-z

[42] S. Phoka, P. Laokul, E. Swatsitang, V. Promarak, S. Seraphin, S. Maensiri, *Mater. Chem. Phys.* **2009**, *115*, 423–428. https://doi.org/10.1016/j.matchemphys.2008.12.031